Chirality-Guided Assembly

DOI: 10.1002/anie.201410768

Chirality-Assisted Ring-Like Aggregation of Aβ(1–40) at Liquid–Solid Interfaces: A Stereoselective Two-Step Assembly Process**

*Guanbin Gao, Mingxi Zhang, Pei Lu, Guanlun Guo, Dong Wang, and Taolei Sun**

Abstract: *Molecular chirality is introduced at liquid–solid interfaces. A ring-like aggregation of amyloid Aβ(1–40) on N-isobutyryl-L-cysteine (L-NIBC)-modified gold substrate occurs at low Aβ(1–40) concentration, while D-NIBC modification only results in rod-like aggregation. Utilizing atomic force microscope controlled tip-enhanced Raman scattering, we directly observe the secondary structure information for Aβ-(1–40) assembly in situ at the nanoscale. D- or L-NIBC on the surface can guide parallel or nonparallel alignment of β-hairpins through a two-step process based on electrostatic-interaction-enhanced adsorption and subsequent stereoselective recognition. Possible electrostatic interaction sites (R5 and K16) and a chiral recognition site (H14) of Aβ(1–40) are proposed, which may provide insight into the understanding of this effect.*

The aggregation and assembly of amyloid peptides at multiple scales may initiate different pathological changes, such as generation of neurotoxic oligomers or formation of insoluble mature fibrils, leading to neurodegenerative diseases.[1] It is generally acknowledged that the typical amyloid fibrils are built by a hairpin-like β-turn (β-hairpin), which stacks into cross-β-sheet structure in a parallel alignment.[2] The concentration of amyloid peptides in vivo is usually several orders of magnitude lower than the threshold for amyloid formation in vitro.[3] A commonly agreed explanation lies in the special role of molecular surface in vivo, for example cytomembrane, which may largely enhance the local concentration of amyloid peptides in the extracellular fluid.[4] Growing evidence has revealed that hydrophobicity, charge, functional groups, and other physical and chemical properties of the interface greatly influence the kinetics of amyloid fibril formation, which dominates the structure and morphology of diverse assembly aggregates.[5] As an intrinsic biochemical signature of life, molecular chirality directly governs the biomolecule recognition process,[6] and it has been extensively reported recently that surface chirality is an important factor determining the behaviors of cells and bio-macromolecules at liquid–solid interfaces.[7] The cytomembrane is mainly composed of phospholipids, which also show distinct asymmetric features owing to high chiral preference of L-enantiomers for phospholipids. Therefore, studying how surface chirality influences amyloid peptide assembly at liquid–solid interfaces, especially at low peptide concentrations, may reveal useful information for comprehensive understanding amyloid formation process in vivo.

Herein we used *N*-isobutyryl cysteine (NIBC)-enantiomer-modified ultra-flat gold substrates to determine the significant influence of surface chirality at the liquid–solid interfaces on Aβ(1–40) assembly at a low concentration of 1 μM. Aβ(1–40) prefers to assemble into a ring-like aggregates on a L-NIBC-modified surface (L-surface), while the corresponding D-surface induces rod-like aggregates. Surface chirality can guide the alignment of β-hairpin in parallel or nonparallel fashions through stereoselective interaction. This leads to the generation of rod-like or ring-like aggregates with different Young's moduli. Utilizing site-specific replacement experiments, we propose the possible electrostatic interaction sites (R5 and K16) and chiral interaction site (H14) of Aβ(1–40). A two-step process of the effect is revealed based on the electrostatic-interaction-enhanced adsorption and subsequent chiral stereoselective interaction, which determines parallel or nonparallel assembly of β-hairpin on a D- or L-surface, respectively.

Aβ(1–40) peptides, which are intrinsically disordered, can experience conformational transition and assemble into dimers, oligomers, fibrils, and other aggregates under different conditions.[8] In a typical in vitro study, Aβ(1–40) peptides can assemble to adopt an orientation at the hydrophobic–hydrophilic interfaces (for example, the air–liquid interface), and then form mature amyloid fibrils freely in buffer solution above the critical micelle concentration (CMC: 17 μM).[9] As shown in the Supporting Information, Figure S1, at low Aβ(1–40) concentrations, such as 1 μM, which are far below the CMC, no fibrils or other assembled aggregates could be found

[*] G. Gao,[+] Prof. M. Zhang,[+] Prof. T. Sun
State Key Laboratory of Advanced Technology for Materials Synthesis and Processing, Wuhan University of Technology
Wuhan 430070 (PR China)
E-mail: suntl@whut.edu.cn

Prof. T. Sun
School of Chemistry, Chemical Engineering and Life Science
Wuhan University of Technology, Wuhan 430070 (PR China)

Dr. P. Lu, Prof. D. Wang
Beijing National Laboratory for Molecular Sciences (BNLMS)
Institute of Chemistry, Chinese Academy of Sciences
Beijing 100190 (PR China)

Dr. G. Guo
Hubei Key Laboratory of Advanced Technology of Automotive Components
Wuhan University of Technology, Wuhan 430070 (PR China)

[+] These authors contributed equally to this work.

[**] This work was supported by National Natural Science Foundation of China (91127027, 51173142, 21105078), the China National Funds for Distinguished Young Scientists (51325302), the Major State Basic Research Development Program of China (973 Program: 2013CB933002), the Program for Changjiang Scholars and Innovative Research Team in University (IRT1169), and the Program of Introducing Talents of Discipline to Universities (B13035).

Supporting information for this article is available on the WWW under http://dx.doi.org/10.1002/anie.201410768.

in solution even at the air–liquid interface. Interestingly, when D(L)-NIBC modified gold surfaces (D(L)-surfaces) were introduced into the solution, a considerable amount of aggregates of Aβ(1–40) could be observed on them even at a concentration of 1 μM. We found that the aggregates on D- and L-surfaces were significantly different. As shown in the atomic force microscope (AFM) image (Figure 1 a–c and Figure S2),

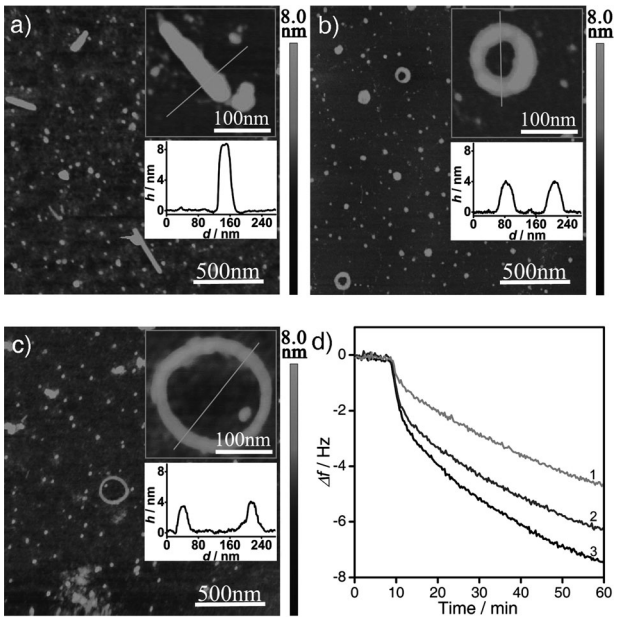

Figure 1. a)–c) AFM images on NIBC-modified gold substrates after incubation in 1 μM Aβ(1–40) solution at 37 °C for 12 h. a) D-surface; b) L-surface; c) (L + D)-surface. Insets: magnified images and section profiles. d) Time-dependent curves of frequency change (Δf) of Aβ(1–40) on D- (curve 1), L- (curve 3), and (L + D)-surfaces (curve 2) in QCM experiments. Flow rates: 120 μL min^{-1} (25 °C).

the D-surface induces the formation of rod-like aggregates after 12 h of incubation in phosphate buffer saline (PBS, 10 μM, pH 7.4) at 37 °C. However, on the corresponding L-surface, rod-like aggregates cannot be observed, while instead a large number of unusual ring-like aggregates appear. A similar phenomenon was also observed on a L/D-NIBC (L/D ratio = 1:1) mixture-modified surface ((L + D)-surface). The statistic data of more than 200 ring-like aggregates show that the ring diameters on the (L + D)-surface (180 ± 30 nm) are significantly larger than those on the L-surface (120 ± 30 nm), but the height (4.0 ± 0.5 nm) of them are almost identical, as revealed by the section profile data. The apparent width observed by AFM is larger than the actual value owing to the probe convolution effect. Detailed statistics (Supporting Information, Table S1) indicate that both aggregates do not exhibit any type of periodic layered stacking as typical mature fibrils do.[10] Previous reports have shown that the presence of air–liquid interface greatly influenced the amyloidosis of α-synuclein at a relatively high concentrations (300 μM).[9d] To clarify its influence on aggregate formation, we investigated the sealed samples without air–liquid interface. Ring-like and rod-like aggregates were also observed on L- and D-surfaces (Supporting Information, Figure S3), indicating that Aβ(1–40) assembly at low concentration is dominated by the liquid–solid interface.

To further explore this phenomenon, we used a quartz-crystal microbalance (QCM) to investigate the adsorption dynamics of Aβ(1–40) on these modified liquid–solid interfaces. D- and L-NIBC-modified QCM resonators were equilibrated with PBS, and then exposed to 1 μM Aβ(1–40) solution with a slow flow rate of 120 μL min^{-1}. As shown in Figure 1 d, the frequency shift on the L-surface is obviously larger than that on the D-surface, and that on the (L + D)-surface lies in a position between them. It suggests that the L-surface has a stronger interaction with Aβ(1–40) than the D-surface. As three modified gold substrates exhibit no evidential difference in wettability and other properties except chirality (Supporting Information, Figure S4), these data indicate that the different adsorption and assembly behaviors should be due to the stereoselective interaction between Aβ(1–40) and the chiral moieties of the surface.

At present, the information about molecular and supramolecular structures of amyloid assemblies is mainly provided by X-ray diffraction (XRD), solid-state nuclear magnetic resonance (SSNMR), electron paramagnetic resonance (EPR), and so on.[11] However, these techniques usually cannot be used for in situ analysis on a surface, especially at a nanoscale. Atomic force microscopy controlled tip-enhanced Raman scattering (AFM-TERS) is a near-field technique combining high spatial resolution of scanning probe microscopy and the chemical information provided by Raman spectroscopy.[12] It is a powerful method to directly characterize the secondary structure of Aβ(1–40) assemblies on surface in a nanoscale, though relevant reports are very rare.[13] Here, the TERS experiment was performed on an integrated AFM-TERS instrument (NTEGRA Spectra, NT-MDT) with upright setup. Each TERS spectrum was collected in different positions along single rod-like aggregates or ring-like aggregates, which contains Raman signals in a nanoscale spot in situ. Representative TERS spectra from rod-like aggregates (curve 1–3) and ring-like aggregates (curve 4–6) are shown in Figure 2 a. In a typical protein Raman spectrum, the amide I region provides main information about polypeptide backbone and intra- and intermolecular hydrogen bonds, which are considered as the characteristic band of the protein secondary structure. Here the second derivative spectra of the amide I region were employed to determine the position of the individual component. As shown in Figure 2 d–e, the peak at 1654 cm^{-1} is assigned to the α-helix, peaks at 1637 and 1645 cm^{-1} are assigned to random coil structures, peaks at 1678, 1685 and 1694 cm^{-1} are assigned as β-turns, and peaks at 1624, 1631, 1663, and 1668 cm^{-1} are assigned as β-sheets.[14] A more detailed description of TERS spectra is provided in the Supporting Information, Table S2. Statistic data show no evidential difference in secondary structure between ring-like aggregates and rod-like aggregates. The existence of β-turn and β-sheet indicates the formation and assembly of β-hairpin. However, the α-helix and random coil peaks of aggregates are stronger than those of mature fibrils (Supporting Information, Figure S5), implying that a well-organized β-sheet structure has not yet formed in both aggregates.

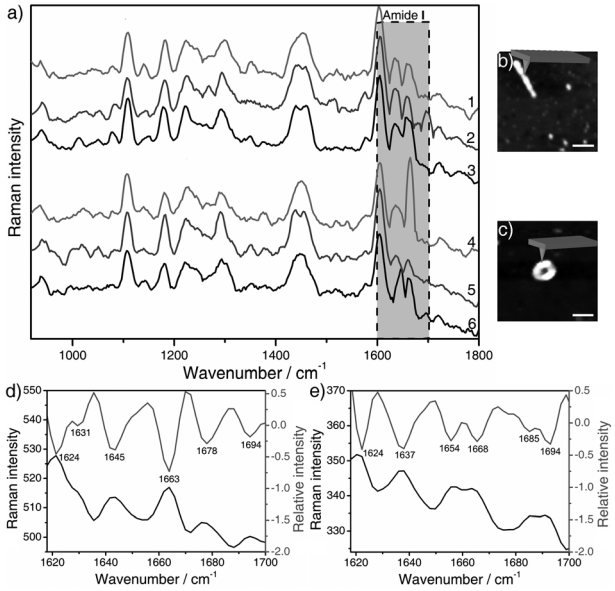

Figure 2. a) Representative TERS spectra of Aβ(1–40) assemblies on NIBC-modified surfaces (curves 1-3: rod-like aggregates; curves 4–6: ring-like aggregates). Amide I regions are marked with a gray band. b),c) Topography images of different aggregates corresponding to the TERS experiment. d),e) Original and second-derivative Raman spectra of amide I regions: d) rod-like aggregates; e) ring-like aggregates. Black: original Raman spectra, gray: second derivative spectra.

The mechanical properties of the Aβ(1–40) aggregates were then characterized by PeakForce QNM (quantitative nanomechanical property mapping) mode on a Bruker Multi-Mode VIII AFM, which allows quantitative nanomechanical mapping of Young's modulus simultaneously (Figure 3, inset) when imaging the topography of samples at high resolution.[15] The modulus images were taken after an absolute calibration process (see the Supporting Information). We randomly selected 10000 spots on ring-like and rod-like aggregates, respectively, and calculated the average Young's modulus and

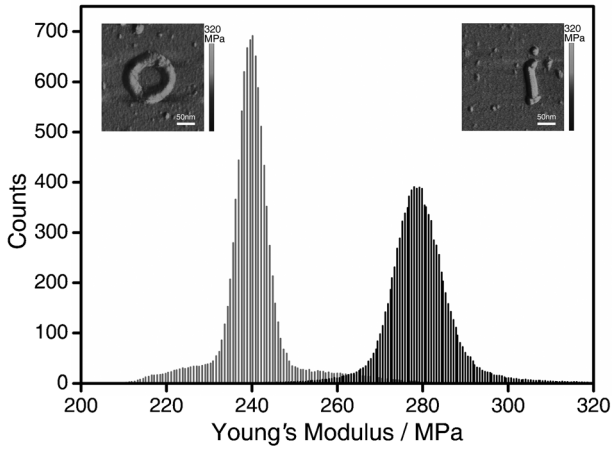

Figure 3. Young's Moduli histograms of ring-like aggregates (gray) and rod-like aggregates (black). Insets: corresponding Young's moduli mapping images of ring-like (left) and rod-like (right) aggregates. Scale bar: 50 nm.

their distribution diagram of each structure. As shown in Figure 3, the average Young's modulus of ring-like aggregates is 239 ± 34 MPa, while the value for rod-like aggregates is 281 ± 38 MPa. Both of them are about one order of magnitude lower than that of typical mature Aβ(1–40) amyloid fibrils.[16] The above results show that the aggregates characteristically have shorter length, lack periodic layered stacking, and have a lower Young's moduli, which is apparently different from typical mature fibrils. Owing to the existence of a β-sheet and a β-turn, both aggregates are may be comparable to amyloid fibril precursors.

The difference in Young's moduli implies a tighter assembly manner of Aβ(1–40) in rod-like aggregates than that in ring-like aggregates,[17] which may be caused by stereospecific interaction of D(L)-NIBC moieties with Aβ(1–40). Previous studies have indicated the importance of pentapeptide fragments in the assembly of Aβ(1–40), for example, Aβ(16-20) KLVFF can act as a self-recognition element during the formation of β-sheet.[18] To get more information, we split Aβ(1–40) into eight pentapeptides, and studied their interactions with D(L)-NIBC by the fluorescent titration method (Supporting Information, Figures S6–S8 and Table S3). Interestingly, the segments containing R (Arg) and K (Lys) residues have obviously higher association constants (K_a) with D(L)-NIBC than others. Considering the ionization effect at physiological conditions (pH ≈ 7.4) and the side-chain properties of Aβ(1–40) (Supporting Information, Table S4), it can be inferred that the deprotonated carboxylate group of D(L)-NIBC may form strong binding with the protonated R5, K16, and K28 residues of Aβ(1–40) by electrostatic interaction, which may contribute greatly to the enhanced adsorption of Aβ(1–40) on the D(L)-NIBC modified liquid–solid interfaces. However, K28 will form a stable salt bridge with D23 (Asp) to form a β-hairpin motif.[19] Therefore, we assume that electrostatic interaction between Aβ(1–40) and D(L)-NIBC may mainly occur on R5 and K16 residues, but not the K28 residue. This has been verified by the K_a value for Aβ(21–30) (hairpin structure can be formed), which is much smaller than those with the K16 residue, for example, Aβ(16–20), Aβ(14–18), and those with the K28 residue but without a hairpin structure (for example Aβ(26–30)).

To further verify this assumption, we adopted site-specific replacement to study the roles of R5 and K16 residues on the adsorption of Aβ(1–40). First, we used G (glycine) to replace both R5 and K16 residues of Aβ(1–40), and incubated the mutant peptide R5G-K16G-Aβ(1–40) with D(L)-NIBC modified gold substrate under the same conditions mentioned above. We found neither ring-like aggregates nor rod-like aggregates of R5G-K16G-Aβ(1–40) on both D- and L-surfaces (Figure 4a,d). Simultaneously, QCM experiments (Figure 4g,h) show that the frequency change of the crystal upon adsorption decreases sharply to less than 1 Hz (nearly within the deviation range of the instrument) on both of them. We then replaced R5 residue only, leaving K16 unchanged (R5G-Aβ(1–40)). Interestingly, we observed rod-like aggregates on the D-surface (Figure 4c) and ring-like aggregates on L-surface (Figure 4f), similar to Aβ(1–40), but the amounts were obviously less. However, when we replaced K16 residue

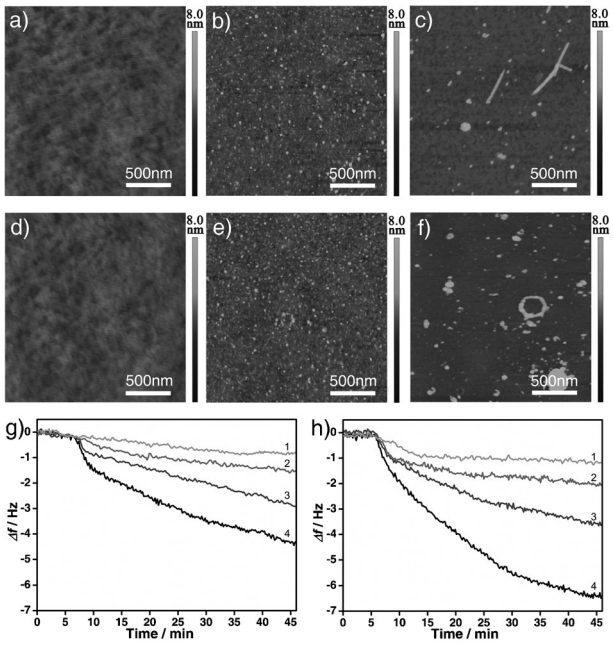

Figure 4. a–f) AFM images of aggregates on a D-surface (a, b, c) and an L-surface (d, e, f) after incubation in 1 μM mutant Aβ(1–40) peptides at 37 °C for 12 h. a),d) R5G-K16G-Aβ(1–40); b),e) K16G-Aβ(1–40); c),f) R5G-Aβ(1–40). Scale bar: 500 nm. g),h) Time-dependent curves of Δf for D- and L-NIBC modified QCM sensors. Curves 1: R5G-K16G-Aβ(1–40); curves 2: K16G-Aβ(1–40); curves 3: R5G-Aβ(1–40); curves 4: Aβ(1–40). Flow rates: 120 μL min^{-1} (25 °C).

only, leaving R5 residue unchanged (K16G-Aβ(1–40)), neither ring-like aggregates nor rod-like aggregates could be observed (Figure 4b,e). Correspondingly, in QCM experiments, the adsorption quantities of both K16G-Aβ(1–40) and R5G-Aβ(1–40) on both D- and L-surfaces were higher than R5G-K16G-Aβ(1–40), but lower than Aβ(1–40). Previous work has indicated that the β-hairpin motif is created by residues 10–40, and residues 1–9 have little connection with Aβ(1–40) assembly.[20] Considering that the R5 residue is in the loop structure (residues 1–9) but not in the β-hairpin motif (residues 10–40), it can be inferred reasonably that the R5 residue only contributes to the adsorption of Aβ(1–40), but has no connection with the assembly of the ring-like and rod-like aggregates. These results not only confirm the significant contribution of R5 and K16 residues to the adsorption of Aβ(1–40), but also reveal another important information that the ring-like aggregates on L-surface may be related to the stereoselective multisite binding with β-hairpin motif.

Based on the above research, it can be reasonably inferred that the K16 residue may play a crucial role on the stereoselective multisite binding and the formation of ring-like aggregates on the L-surface. To investigate this hypothesis, we used molecular docking and structure optimization to simulate the orientation of D(L)-NIBC enantiomers relative to K16 and other residues of Aβ(1–40) near it. As shown in the Supporting Information, Figure S9, both D- and L-NIBC have similar electrostatic interactions via the amino group of K16 residue and the carboxyl group of NIBC. However, interestingly, obviously different binding behaviors are observed for the nearby H14 residue, which shows moderate H-bonding interaction (bond length ca. 2.6 Å) with L-NIBC but negligible interaction with D-NIBC. This reveals that the H14 residue may act as a chiral recognition site, working together with the K16 residue, to give an advantageous conformation that can fit well with L-NIBC moiety but mismatch with D-NIBC.

Furthermore, we used site-specific replacement to study the roles of H14 and K16 residues on the formation of ring-like aggregates. First, we used G (glycine) to replace both K16 and H14 residues of Aβ(1–40), and incubated the mutant peptide H14G-K16G-Aβ(1–40) with L(D)-NIBC modified surfaces under the same conditions mentioned above. We found that neither rod-like aggregates nor ring-like aggregates of H14G-K16G-Aβ(1–40) were formed on both D- and L-surfaces (Supporting Information, Figure S10a,c). However, when we replaced H14 residue only, leaving K16 unchanged (H14G-Aβ(1–40)), we observed rod-like aggregates on both surfaces (Supporting Information, Figure S10b,d), but no ring-like aggregates could be found. These results confirm the cooperative effect of H14 and K16 residues on the stereoselective interaction between Aβ(1–40) and L(D)-NIBC modification and the formation of ring-like aggregates on the L-surface.

The above analysis reveals a possible two-step process for chirality-assisted ring-like or rod-like aggregation of Aβ(1–40) at liquid–solid interfaces: R5 and K16 residues contribute greatly to the enhanced adsorption of Aβ(1–40) owing to electrostatic interactions, largely improving the local concentration, which is a prerequisite condition for Aβ(1–40) assembly; the H14 residue acts as the chiral recognition center with the aid of K16 residue. Though such stereoselective interactions caused by chirality are too weak to affect the β-hairpin stacking into a β-sheet, they can guide the stacking manner of β-hairpin in different aggregates. Considering that the L-NIBC moiety can form H-bonding and electrostatic interaction simultaneously with H14 and K16 residues, it may intercalate into two adjacent β-hairpin structures and break the parallel alignment of them,[2,21] resulting in a non-parallel alignment mode (Supporting Information, Figure S11). However, on the D-surface, the alignment of Aβ(1–40) remains a parallel mode because the interaction between Aβ(1–40) and D-NIBC moiety is weak. The parallel or nonparallel alignment has no influence on the β-sheet structure, but will change the morphology and mechanical property of observed assemblies, resulting in rod-like or ring-like aggregates with different Young's moduli. Moreover, the surface density of L-NIBC has obvious impact on the curvature of the non-parallel alignment, which leads to a size difference between ring-like aggregates on L- and (L + D)-surfaces. This assumption has been confirmed at least partially by the AFM images taken from different regions in one sample (Figure 5), which clearly demonstrate different stages of ring-like aggregate formation. Recent work by Jordens et al. illustrates a spontaneous curvature of β-lactoglobulin fibrils at air–water and oil–water interfaces, which also leads to ring-like conformation.[22] They confirm that this process is governed by the interaction between chiral filaments and the interface. This work and our findings share one important aspect: chirality of either the

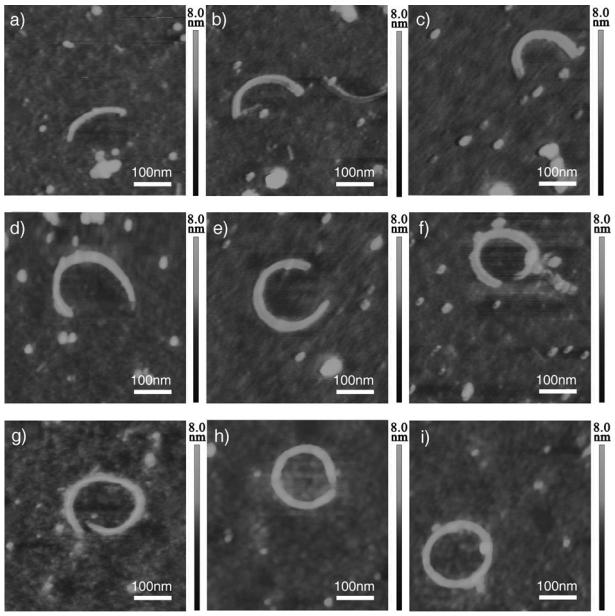

Figure 5. AFM images taken from different regions of an (L + D)-surface after incubation in Aβ(1–40) solution (1 μM in PBS) at 37 °C for 12 h.

interfaces or the filaments can break the symmetry by stereoselective interactions and induce spontaneous curvature of amyloid fibrils adsorbing on surface.

In summary, we have shown how surface chirality influences the assembly of Aβ(1–40) at low concentrations. TERS experiment indicates that ring-like aggregates have similar secondary structure to rod-like aggregates of Aβ(1–40). Their different β-hairpin alignment modes are determined by surface chirality through electrostatic-interaction-enhanced stereoselective recognition. On the basis of experimental and theoretical study, we also propose the electrostatic interaction sites (R5 and K16) and chiral recognition site (H14) on Aβ(1–40). These results provide interesting insight to reconsider the aggregation mechanism of amyloid precursors on biological membranes at low concentrations, which may lead to innovation in therapeutics of neurodegenerative diseases.

Received: November 5, 2014
Revised: November 29, 2014
Published online: December 22, 2014

Keywords: amyloids · chirality · stereoselectivity · surface assembly · surface interactions

[1] a) C. M. Dobson, *Trends Biochem. Sci.* **1999**, *24*, 329–332; b) D. J. Selkoe, *Physiol. Rev.* **2001**, *81*, 741–766; c) J. Hardy, D. J. Selkoe, *Science* **2002**, *297*, 353–356; d) C. M. Dobson, *Nature* **2003**, *426*, 884–890; e) J. P. Cleary, D. M. Walsh, J. J. Hofmeister, G. M. Shankar, M. A. Kuskowski, D. J. Selkoe, K. H. Ashe, *Nat. Neurosci.* **2005**, *8*, 79–84.

[2] a) T. Lührs, C. Ritter, M. Adrian, D. Riek-Loher, B. Bohrmann, H. Döbeli, D. Schubert, R. Riek, *Proc. Natl. Acad. Sci. USA* **2005**, *102*, 17342–17347; b) N. Mousseau, P. Derreumaux, *Acc. Chem. Res.* **2005**, *38*, 885–891; c) T. Eichner, E. R. Sheena, *Mol. Cell* **2011**, *43*, 8–18; d) L. Larini, J. E. Shea, *Biophys. J.* **2012**, *103*, 576–586; e) R. Tycko, R. B. Wickner, *Acc. Chem. Res.* **2013**, *46*, 1487–1496.

[3] a) C. Haass, M. G. Schlossmacher, A. Y. Hung, C. V. Pelfrey, A. Mellon, B. L. Ostaszewski, I. Lieberburg, E. H. Koo, D. Schenk, D. B. Teplow, D. J. Selkoe, *Nature* **1992**, *359*, 322–325; b) R. Sabaté, J. Estelrich, *J. Phys. Chem. B* **2005**, *109*, 11027–11032; c) L. Shen, T. Adachi, D. V. Bout, X. Y. Zhu, *J. Am. Chem. Soc.* **2012**, *134*, 14172–14178.

[4] a) M. Zhu, P. O. Souillac, C. Ionescu-Zanetti, S. A. Carter, A. L. Fink, *J. Biol. Chem.* **2002**, *277*, 50914–50922; b) M. F. M. Engel, C. C. VandenAkker, M. Schleeger, K. P. Velikov, G. H. Koenderink, M. Bonn, *J. Am. Chem. Soc.* **2012**, *134*, 14781–14788; c) M. F. M. Sciacca, J. R. Brender, D. K. Lee, A. Ramamoorthy, *Biochemistry* **2012**, *51*, 7676–7684; d) M. F. M. Sciacca, S. A. Kotler, J. R. Brender, J. Chen, D. K. Lee, A. Ramamoorthy, *Biophys. J.* **2012**, *103*, 702–710; e) S. A. Kotler, P. Walsh, J. R. Brender, A. Ramamoorthy, *Chem. Soc. Rev.* **2014**, *43*, 6692–6700.

[5] a) I. W. Hamley, *Nat. Chem.* **2010**, *2*, 707–708; b) B. Moores, E. Drolle, S. J. Attwood, J. Simons, Z. Leonenko, *PLoS One* **2011**, *6*, e25954; c) A. Keller, M. Fritzsche, Y. P. Yu, Q. Liu, Y. M. Li, M. Dong, F. Besenbacher, *ACS Nano* **2011**, *5*, 2770–2778; d) Q. Wang, N. Shah, J. Zhao, C. Wang, C. Zhao, L. Liu, L. Li, F. Zhou, J. Zheng, *Phys. Chem. Chem. Phys.* **2011**, *13*, 15200–15210.

[6] a) W. A. Bonner, *Origins Life Evol. Biospheres* **1991**, *21*, 59–111; b) A. Berthod, *Anal. Chem.* **2006**, *78*, 2093–2099; c) J. Zhang, M. Zhang, K. Tang, F. Verpoort, T. Sun, *Small* **2014**, *10*, 32–46.

[7] a) M. Geva, F. Frolow, M. Eisenstein, L. Addadi, *J. Am. Chem. Soc.* **2003**, *125*, 696–704; b) T. Sun, D. Han, K. Rhemann, L. Chi, H. Fuchs, *J. Am. Chem. Soc.* **2007**, *129*, 1496–1497; c) K. Tang, H. Gan, Y. Li, L. Chi, T. Sun, H. Fuchs, *J. Am. Chem. Soc.* **2008**, *130*, 11284–11285; d) H. Gan, K. Tang, T. Sun, M. Hirtz, Y. Li, L. Chi, S. Butz, H. Fuchs, *Angew. Chem. Int. Ed.* **2009**, *48*, 5282–5286; *Angew. Chem.* **2009**, *121*, 5386–5390; e) X. Wang, H. Gan, T. Sun, *Adv. Funct. Mater.* **2011**, *21*, 3276–3281; f) G. Qing, T. Sun, *Adv. Mater.* **2011**, *23*, 1615–1620; g) M. Zhang, G. Qing, T. Sun, *Chem. Soc. Rev.* **2012**, *41*, 1972–1984; h) G. Qing, T. Sun, *NPG Asia Mater.* **2012**, *4*, e4; i) G. Qing, S. Zhao, Y. Xiong, Z. Lv, F. Jiang, Y. Liu, H. Chen, M. Zhang, T. Sun, *J. Am. Chem. Soc.* **2014**, *136*, 10736–10742.

[8] a) A. Lomakin, D. S. Chung, G. B. Benedek, D. A. Kirschner, D. B. Teplow, *Proc. Natl. Acad. Sci. USA* **1996**, *93*, 1125–1129; b) F. Chiti, C. M. Dobson, *Annu. Rev. Biochem.* **2006**, *75*, 333–366.

[9] a) R. Wetzel, *Acc. Chem. Res.* **2006**, *39*, 671–679; b) S. Vivekanandan, J. R. Brender, S. Y. Lee, A. Ramamoorthy, *Biochem. Biophys. Res. Commun.* **2011**, *411*, 312–316; c) I. W. Hamley, *Chem. Rev.* **2012**, *112*, 5147–5192; d) S. Campioni, G. Carret, S. Jordens, L. Nicoud, R. Mezzenga, R. Riek, *J. Am. Chem. Soc.* **2014**, *136*, 2866–2875.

[10] a) M. Schmidt, C. Sachse, W. Richter, C. Xu, M. Fändrich, N. Grigorieff, *Proc. Natl. Acad. Sci. USA* **2009**, *106*, 19813–19818; b) Y. Miller, B. Y. Ma, R. Nussinov, *Chem. Rev.* **2010**, *110*, 4820–4838.

[11] a) E. D. Eanes, G. G. Glenner, *J. Histochem. Cytochem.* **1968**, *16*, 673–677; b) J. J. Balbach, A. T. Petkova, N. A. Oyler, O. N. Antzutkin, D. J. Gordon, S. C. Meredith, R. Tycko, *Biophys. J.* **2002**, *83*, 1205–1216; c) R. Tycko, *Biochemistry* **2003**, *42*, 3151–3159; d) M. Margittai, R. Langen, *Q. Rev. Biophys.* **2008**, *41*, 265–297.

[12] a) E. Bailo, V. Deckert, *Chem. Soc. Rev.* **2008**, *37*, 921–930; b) T. Schmid, L. Opilik, C. Blum, R. Zenobi, *Angew. Chem. Int. Ed.* **2013**, *52*, 5940–5954; *Angew. Chem.* **2013**, *125*, 6054–6070.

[13] a) E. Bailo, V. Deckert, *Angew. Chem. Int. Ed.* **2008**, *47*, 1658 – 1661; *Angew. Chem.* **2008**, *120*, 1682 – 1685; b) D. Kurouski, S. Zaleski, F. Casadio, R. P. V. Duyne, N. C. Shah, *J. Am. Chem. Soc.* **2014**, *136*, 8677 – 8684.

[14] a) D. M. Byler, H. Susi, *J. Ind. Microbiol. Biotechnol.* **1988**, *3*, 73 – 88; b) N. C. Maiti, M. M. Apetri, M. G. Zagorski, P. R. Carey, V. E. Anderson, *J. Am. Chem. Soc.* **2004**, *126*, 2399 – 2408; c) D. Kurouski, T. Deckert-Gaudig, V. Deckert, I. K. Lednev, *J. Am. Chem. Soc.* **2012**, *134*, 13323 – 13329; d) M. Paulite, C. Blum, T. Schmid, L. Opilik, K. Eyer, G. C. Walker, R. Zenobi, *ACS Nano* **2013**, *7*, 911 – 920.

[15] a) J. Adamcik, A. Berquand, R. Mezzenga, *Appl. Phys. Lett.* **2011**, *98*, 193701 – 193703; b) H. Liu, N. Chen, S. Fujinami, D. Louzguine-Luzgin, K. Nakajima, T. Nishi, *Macromolecules* **2012**, *45*, 8770 – 8779.

[16] a) T. P. Knowles, A. W. Fitzpatrick, S. Meehan, H. R. Mott, M. Vendruscolo, C. M. Dobson, M. E. Welland, *Science* **2007**, *318*, 1900 – 1903; b) T. P. Knowles, MJ. Buehler, *Nat. Nanotechnol.* **2011**, *6*, 469 – 479; c) J. Adamcik, C. Lara, I. Usov, J. S. Jeong, F. S. Ruggeri, G. Dietler, H. A. Lashuel, I. W. Hamleyd, R. Mezzenga, *Nanoscale* **2012**, *4*, 4426 – 4429.

[17] a) R. Paparcone, S. Keten, MJ. Buehler, *J. Biomechnol.* **2010**, *43*, 1196 – 1201; b) J. Adamcik, R. Mezzenga, *Curr. Opin. Colloid Interface Sci.* **2012**, *17*, 369 – 376.

[18] a) L. O. Tjernberg, J. Näslund, F. Lindqvist, J. Johansson, A. R. Karlström, J. Thyberg, L. Terenius, C. Nordstedt, *J. Biol. Chem.* **1996**, *271*, 8545 – 8548; b) W. P. Esler, E. R. Stimson, J. R. Ghilardi, Y.-A. Lu, A. M. Felix, H. V. Vinters, P. W. Mantyh, J. P. Lee, J. E. Maggio, *Biochemistry* **1996**, *35*, 13914 – 13921; c) M. J. Krysmann, V. Castelletto, A. Kelarakis, I. W. Hamley, R. A. Hule, D. J. Pochan, *Biochemistry* **2008**, *47*, 4597 – 4605.

[19] a) A. T. Petkova, R. D. Leapman, Z. H. Guo, W. M. Yau, M. P. Mattson, R. Tycko, *Science* **2005**, *307*, 262 – 265; b) K. L. Sciarretta, D. J. Gordon, A. T. Petkova, R. Tycko, S. C. Meredith, *Biochemistry* **2005**, *44*, 6003 – 6014.

[20] a) A. T. Petkova, W.-M. Yau, R. Tycko, *Biochemistry* **2006**, *45*, 498 – 512; b) T. Takeda, D. K. Klimov, *J. Phys. Chem. B* **2009**, *113*, 11848 – 11857.

[21] a) A. T. Petkova, Y. Ishii, J. J. Balbach, O. N. Antzutkin, R. D. Leapman, F. Delaglio, A. R. Tycko, *Proc. Natl. Acad. Sci. USA* **2002**, *99*, 16742 – 16747; b) R. Paparcone, M. A. Pires, M. J. Buehler, *Biochemistry* **2010**, *49*, 8967 – 8977.

[22] S. Jordens, E. E. Riley, I. Usov, L. Isa, P. D. Olmsted, R. Mezzenga, *ACS Nano* **2014**, *8*, 11071 – 11079.

